

Nonlinear theory of a folded waveguide gyrotron traveling-wave tube amplifier

A. K. Ganguly* and J. J. Choi†

Naval Research Laboratory, Washington, D.C. 20375

C. M. Armstrong

Northrop Grumman Corporation, Rolling Meadows, Illinois 60008

(Received 14 June 1995)

We have developed a three-dimensional nonlinear theory for broadband gyrotron traveling-wave amplification in an H -plane-bend folded waveguide. The H -plane-bend configuration is formed by folding a rectangular waveguide so that the orientation of the magnetic field changes along the bend in contrast to the conventional E -plane bend, where the orientation of the electric field changes. Calculations show the feasibility of amplifier operation with large instantaneous bandwidth and moderate efficiency both in the slow wave region and the reduced dispersion fast wave region. Numerical results for a cold beam show an efficiency of 26% with 11% bandwidth in the slow wave region and an efficiency of 47% with 10% bandwidth in the fast wave region. For an electron beam with 2% velocity spread and 2% guiding center spread, the slow wave efficiency drops to 6% but the bandwidth increases to 16% whereas the efficiency and bandwidth of the fast waves decrease by a small amount to 42% and 9.5%, respectively. The efficiency is more sensitive to the axial beam velocity spread in the slow wave region due to larger Doppler shift.

PACS number(s): 52.75.Ms, 42.52.+x, 85.10.Jz

I. INTRODUCTION

Development of a high power (10–100 kW) millimeter wave amplifier (30–120 GHz) with broad instantaneous bandwidth ($> 15\%$) operating at moderate beam voltage (< 60 kV) is a critical issue in many applications such as high resolution radar, satellite communications, millimeter wave imaging, and material processing. Conventional approaches for achieving wideband radiation amplification in the gyrodevices are (a) reduced dispersion interaction circuits, e.g., waveguides loaded with dielectric [1] or periodic metal discs [2] or periodic metal posts [3]; and (b) a tapered distributed amplifier circuit in a nonlinearly tapered magnetic field [4,5]. An experiment [6] with a two-stage tapered gyrotron traveling wave amplifier in the K_a band has shown a bandwidth of 20% at an efficiency of 15%, and a 25-dB saturated gain in agreement with theory. In this device, a precise control of the guide magnetic field profile is required over the entire interaction length. Theoretical predictions for the bandwidth in a dielectric-lined waveguide are, respectively, 28% in the slow wave region [1] and 20% in the fast wave region [7] of the frequency spectrum. In an experiment with the fast waves in a dielectric-loaded waveguide, Leou *et al.* [8] have measured a bandwidth of 11% in the X band at an efficiency of 11% and 27-dB saturated gain. Large bandwidth ($> 20\%$) amplification

has been demonstrated in slow wave devices but at lower efficiency and power compared to the fast wave devices. A low power (~ 100 W) broadband amplifier in the 40–54-GHz frequency range (bandwidth $> 25\%$) was developed by Dohler, Gallagher, and Richards [9] using a linear beam interaction in a slow wave circuit formed with an E -plane-bend folded rectangular waveguide. The saturated gain was found to be 30 dB. In the E -plane bend, the orientation of the electric field of the fundamental TE_{10} (transverse electric) mode changes as the wave propagates along the bend.

In order to enhance the power handling capability of a folded waveguide, gyrotron traveling-wave interaction in an H -plane-bend configuration was proposed [10]. The slots for beam propagation in an E -plane-bend folded guide are in planes normal to the electric field, and the openings are small to reduce perturbation of the empty waveguide modes. The small diameter of the beam limits the current and the power flow in the device. The H -plane-bend circuit, on the other hand, is formed by bending a rectangular waveguide in a plane so that the orientation of the TE_{10} magnetic field changes and the beam tunnel passes through the walls of the waveguide which are parallel to the electric field. In this case, the slots for beam propagation can be made larger with little distortion of the field structure. The large beam current and stronger interaction of a gyrating electron beam produce higher output power compared to the linear beam E -plane-bend device. The folded waveguide gyrotron traveling-wave tube (gyro-TWT) has some advantages over other broadband gyrotron devices [1–5]. In the folded waveguide, the spent electron beam is naturally separated from the radiation. Therefore, it is simpler to

*Permanent address: Omega-P Inc., 2008 Yale Station, New Haven, CT 06520.

†Permanent address: Science Applications International Co., McLean, VA 22102.

design input and output couplers, and depressed collector techniques for efficiency enhancement can be easily applied.

We consider both smooth and double-ridged folded waveguides. The separation of the spatial harmonics is wider in the folded ridged waveguide, and operation at a broader bandwidth is possible in such interaction circuits. A linear theory [11] of the slow wave cyclotron interaction in a folded rectangular waveguide with H -plane bend was developed to calculate the linear gain and bandwidth of the device. The magnetic field of the radiation field was not included in the calculation. To obtain the correct bandwidth in a slow wave cyclotron interaction, the contributions to the beam-wave coupling from both the electric and magnetic fields of radiation have to be considered, since the frequency range of interest spans the intersection of the light line with the waveguide dispersion curves. In this paper, we develop a three-dimensional, self-consistent nonlinear theory for the interaction of a gyrating electron beam with the radiation field in a folded waveguide and calculate the saturated efficiency, gain, and bandwidth. All components of the electromagnetic field are included in the interaction process.

A brief discussion of the TE_{10} -mode structure in a double-ridged rectangular waveguide is given in Sec. II. Detailed analyses of the waveguide characteristics can be found in Refs. [12,13]. The wave propagation in the folded configuration is treated under the approximations commonly employed in the literature [14]. It is assumed that the mode structure is not altered in the folded guide, but that the axial phase velocity decreases due to propagation along a circuitous path. The drift motion of the electrons is along the z axis, and interaction with the wave field occurs as the beam successively passes through the legs of the bend separated by a distance l along the z axis (Fig. 1). The field along the electron orbits are, therefore, not sinusoidal but periodic with a periodicity,

l . In Sec. III, the slow-time-scale equations for electron motion and the evolution of the electromagnetic field are derived. These equations are similar to the steady-state models used in other gyrotron devices [15]. Numerical results for some specific design parameters are given in Sec. IV.

II. DISPERSION CHARACTERISTICS OF H-PLANE-BEND FOLDED WAVEGUIDES

A schematic of the folded waveguide interaction circuit is shown in Fig. 1(a), and the parameters of the double-ridged waveguide cross-section are shown in Fig. 1(b). In keeping with common practice, the ridged guide modes are given the same designations as the corresponding modes in the rectangular waveguide. It is assumed that a TE_{10} mode propagates along the folded path z' shown by a dotted line, and that the electron beam travels along the z axis through holes in the waveguide walls which are parallel to the wave electric field. The phase velocity ($v_{ph}^{(0)}$) of the wave at an angular frequency ω and propagation constant κ_0 along the serpentine path is the same as in a straight waveguide, and may be written as

$$v_{ph}^{(0)} = \omega / \kappa_0, \quad (1)$$

where $\omega^2 = \omega_c^2 + c^2 \kappa_0^2$. The cutoff frequency ω_c of the TE_{10} mode is given by the lowest root of the following equation [12,13]:

$$\tan(k_c a_0 / 2) - \frac{b_0}{b} \cos\left(k_c \frac{a - a_0}{2}\right) + \left(\frac{\mu_0}{\epsilon_0}\right)^{1/2} \frac{b_0}{b} B_c = 0, \quad (2)$$

where $k_c = \omega_c / c$, $c = \sqrt{1/\mu_0 \epsilon_0}$ is the velocity of light in vacuum, and ϵ_0 and μ_0 , respectively, are the vacuum dielectric constant and permittivity. The susceptance term B_c represents the effect of the step discontinuity at $x = \pm a_0/2$. The values for B_c may be found in the *Waveguide Handbook* [16]. An approximate form [17] for B_c is shown by

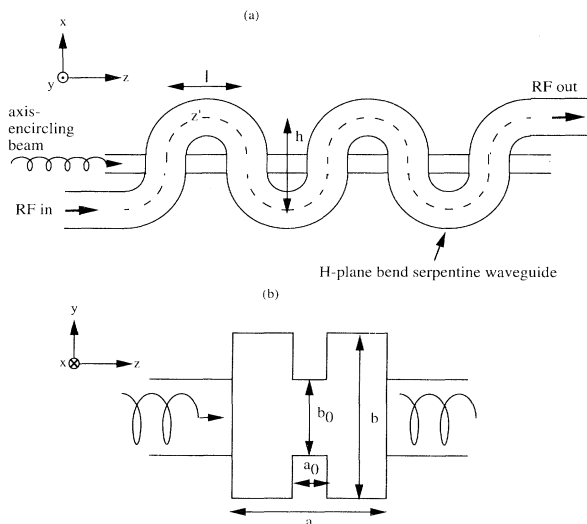


FIG. 1. (a) Schematic of an H -bend folded waveguide. (b) Cross-sectional view in the yz plane of a leg traversed by the electron beam in a double-ridged rectangular waveguide.

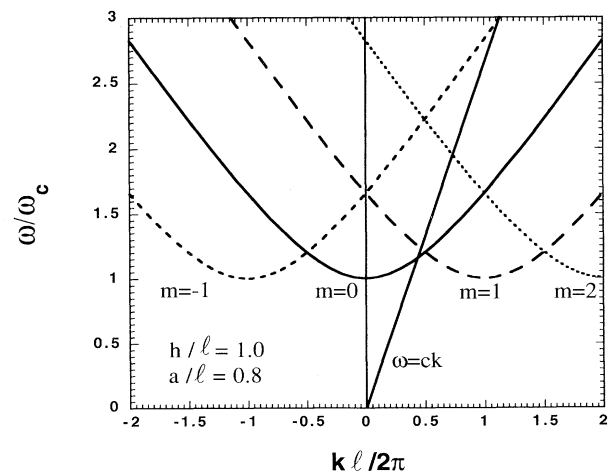


FIG. 2. Dispersion curves for the circuit of Fig. 1.

$$\left(\frac{\mu_0}{\epsilon_0}\right)^{1/2} B_c = \frac{2}{\pi} k_c b \ln \left[\csc \left[\frac{\pi b}{2b_0} \right] \right]. \quad (3)$$

Although the phase velocity of the wave along the folded path is $v_{ph}^{(0)}$, it can be seen from Fig. 1 that electrons moving in the z direction experience a wave traveling with an effective phase velocity v_{ph} and unperturbed axial wave vector k_0 given by

$$\begin{aligned} v_{ph} &= \frac{l}{l+h} v_{ph}^{(0)}, \\ k_0 &= \frac{l+h}{l} k_0. \end{aligned} \quad (4)$$

Accordingly, the unperturbed rf field in a folded waveguide is assumed to be similar to the field in an equivalent straight waveguide [14] where the phase velocity is lowered by a factor of $l/(l+h)$. Hence the axial and temporal variation of the traveling wave is represented by $e^{i\{\omega t - [l/(l+h)]kz\}}$, and the unperturbed dispersion

relation for the fundamental space harmonic ($m=0$) becomes

$$\omega = \left\{ \omega_c^2 + \left[\frac{l}{l+h} \right]^2 (ck_0)^2 \right\}^{1/2}. \quad (5)$$

The frequencies of higher space harmonics may be written as

$$\omega = \left\{ \omega_c^2 + \left[\frac{l}{l+h} \right]^2 c^2 \left[k_{0,m} - \frac{2\pi m}{l} \right]^2 \right\}^{1/2}, \quad (6)$$

where $k_{0,m} = k_0 + 2m\pi/l$ is the phase constant of the m th space harmonic. The unperturbed phase constants will be denoted by a superscript 0. The frequency of the TE₁₀ mode as a function of the wave vector is plotted in Fig. 2.

The dominant contribution to the radiation field components of the TE₁₀ mode in a double-ridged waveguide may be expressed as [12,13]

$$E_y = \frac{m_0 c^2}{ea} e_t(x) F(z) e^{i\omega t}, \quad (7)$$

$$e_t(x) = \frac{1}{N} \begin{cases} \cos(k_c |x|), & 0 < |x| < a_0/2 \\ \frac{b_0}{b} \frac{\cos(k_c a_0/2)}{\sin[k_c(a-a_0)/2]} \sin \left[k_c \left[\frac{a}{2} - |x| \right] \right], & a_0/2 < |x| < a/2, \end{cases} \quad (8)$$

$$N^2 = \frac{a_0 b_0}{2a^2} \left\{ \left[1 + \frac{\sin(2\xi_0)}{2\xi_0} \right] + \frac{b_0(a-a_0)}{ba_0} \frac{\cos^2 \xi_0}{\sin^2 \xi_1} \left[1 - \frac{\sin(2\xi_1)}{2\xi_1} \right] \right\}, \quad (9)$$

$$F(z) = A(z) e^{-i[l/(l+h)]\xi z} = A(z) e^{-[il/(l+h)] \int_0^z k(z') dz'}, \quad (10)$$

$$H_x = -\frac{i}{\mu_0 \omega} \frac{\partial E_y}{\partial z}, \quad (11)$$

$$H_z = \frac{i}{\mu_0 \omega} \frac{\partial E_y}{\partial x}. \quad (12)$$

For a tenuous electron beam, the amplitude $A(z)$ and the axial wave vector $k(z)$ in Eq. (10) are assumed to vary slowly along the axis, i.e., $\lambda_z dA/dz \ll A$, and $\lambda_z dk/dz \ll k$. To be exact, the field components in a waveguide with step discontinuity have to be expressed as a linear superposition of orthonormal basis functions to satisfy boundary conditions at the discontinuity. The effects of the fringing fields are taken into account in the dispersion relation by including the susceptance term in Eq. (2). Since the electron orbits are not close to the fringing fields, we use the approximate fields in Eqs. (7)–(9) to calculate the beam-wave coupling parameter. The normalization constant N in Eq. (9) is chosen such that

$$\int_{-a/2}^{a/2} d(x/a) \int_{-b/2}^{b/2} d(y/a) [e_t(x)]^2 = 1.$$

The power in the z direction can be obtained from the Poynting flux $P = \frac{1}{2} \text{Re} \int (\mathbf{E} \times \mathbf{H}^*) \cdot \hat{\mathbf{e}}_z dS$, and using Eqs. (7) and (8) we obtain

$$P = \frac{1}{2} \frac{\epsilon_0 m_0^2 c^5}{e^2} \frac{ck}{\omega(1+h/l)} A^2(z). \quad (13)$$

In Eq. (9), $\xi_0 = k_c a_0/2$ and $\xi_1 = k_c(a-a_0)/2$. The results for the unridged waveguide are obtained in the limits $a_0 \rightarrow a$, $b_0 \rightarrow b$, and $k_c \rightarrow \pi/a$.

III. SLOW TIME SCALE FORMULATION

The self-consistent evolution of the radiation field and the trajectories of an ensemble of electrons can be calculated from a simultaneous solution of Maxwell's equations and the Lorentz force equation

$$\nabla^2 \mathbf{E} - \mu_0 \epsilon_0 \frac{\partial^2 \mathbf{E}}{\partial t^2} = \mu_0 \frac{\partial \mathbf{J}}{\partial t}, \quad (14)$$

$$\frac{d}{dt} (\gamma \mathbf{v}) = -\frac{e}{m_0} (\mathbf{v} \times \mathbf{B}_0) - \frac{e}{m_0} (\mathbf{E} + \mathbf{v} \times \mathbf{B}), \quad (15)$$

where \mathbf{B}_0 is the axial guide magnetic field, and \mathbf{E} and \mathbf{B}

are the radiation electric and magnetic fields, respectively. The axial guide magnetic field may be weakly nonuniform, and is written as

$$\mathbf{B}_0(x, y, z) = B_{0z}(z)\hat{\mathbf{e}}_z - \frac{1}{2} \left[\frac{\partial B_{0z}}{\partial z} \right] (x\hat{\mathbf{e}}_x + y\hat{\mathbf{e}}_y).$$

The slow-time-scale equations for the radiation field can be obtained in the usual way [15] by taking the dot product of \mathbf{E} with Eq. (14), integrating over the cross section of the waveguide and averaging over a period of the wave. The resulting equations are

$$\left\{ \frac{\partial^2 A}{\partial z^2} - \frac{l^2}{(l+h)^2} \left[\frac{\partial \xi}{\partial z} \right]^2 A + \left[\frac{\omega^2}{c^2} - k_c^2 \right] A \right\} - i \frac{l}{l+h} \left\{ 2 \frac{\partial \xi}{\partial z} \frac{\partial A}{\partial z} + \frac{\partial^2 \xi}{\partial z^2} A \right\} = i\mu_0\omega \int_0^{2\pi} \frac{d(\omega t)}{2\pi} \int \int_{S_b} dx dy \{ j_y(z, t) + j_y^*(z, t) \} \frac{e^2 E_y^*}{m_0^2 c^4 A} e^{-i\omega t}, \quad (16)$$

S_b is the cross-sectional area of the beam. The current density [15] can be written as

$$\mathbf{j}(\mathbf{r}, t) = -I_0 \int f_0(\mathbf{v}) d\mathbf{v} \int \int_{S_b} \frac{dx_0 dy_0}{S_b} \int_{-T/2}^{T/2} dt_0 \sigma_{\perp}(t_0) \sigma_{\parallel}(x_0, y_0) \frac{v_z}{\langle v_{z0} \rangle} \times \frac{\mathbf{v}(x, y, z, t)}{|v_z(\mathbf{x}, t, z; \mathbf{x}_0, t_0)|} \delta(x - x(\mathbf{x}_0, t_0, z)) \delta(y - y(\mathbf{x}_0, t_0, z)) \delta(t - t(\mathbf{x}_0, t_0, z)), \quad (17)$$

where $v(\mathbf{x}, t, z; \mathbf{x}_0, t_0)$ is the velocity of an electron at axial position z with transverse position $\mathbf{x} = (x, y)$ which entered the waveguide at $z=0$ at time t_0 with transverse positions $\mathbf{x}_0 = (x_0, y_0)$, $t(z; x_0, y_0, t_0) = t_0 + \int_0^z dz' / v_z(z'; x_0, y_0, t_0)$, and $T = L / v_z$, L being the length of the interaction region. The electronic current is $I_0 = n_0 e \langle v_{z0} \rangle S_b$, where n_0 is the average electron density and $\langle v_{z0} \rangle$ is the axial velocity of electrons at $z=0$. The initial distribution of the electrons in cross section, phase, and velocity are described, respectively, by σ_{\perp} , σ_{\parallel} , and $f_{0(\mathbf{v})}$, subject to the normalization

$$\int f_0(\mathbf{v}) d\mathbf{v} = 1, \quad \int_{S_b} \sigma_{\perp}(x_0, y_0) dx_0 dy_0 = S_b, \quad \int_{-T/2}^{T/2} \sigma_{\parallel}(t_0) dt_0 = T.$$

The conductive losses in the waveguide walls can be accounted for by replacing the term ω^2/c^2 in Eq. (16) by $\omega^2(1 - i \tan \delta_l)/c^2$, where $\tan \delta_l$ is the loss tangent of the circuit. This replacement models the propagation of the waves in a lossy medium with a complex dielectric constant $\epsilon = \epsilon_0(1 - i \tan \delta_l)$. The loss tangent can be expressed in terms of the attenuation coefficient Γ_a of the waves:

$$\tan \delta_l = 2(\Gamma_a c / \omega) \sqrt{1 - (\omega_c / \omega)^2}.$$

Γ_a for the TE₁₀ mode in a double-ridged waveguide may be calculated from the approximate formula [13]

$$\Gamma_a = \frac{\xi}{b_0} \left[\frac{\epsilon_0 \omega_c}{2\sigma} \right]^{1/2} \frac{\pi}{k_c a} \left\{ \sin \xi_0 + \frac{b_0}{b} \cos \xi_1 \tan(\xi_1/2) \right\} \left[\frac{\omega}{\omega_c} \right]^{1/2} \frac{1 + \frac{2b}{a} \left[\frac{\omega_c}{\omega} \right]^2}{\left[1 - \left[\frac{\omega_c}{\omega} \right]^2 \right]^{1/2}} \text{cm}^{-1}, \quad (18)$$

where σ is the conductivity, b_0 is in centimeters, and ξ is a correction constant slightly larger than unity ($1.0 < \xi < 1.5$). The correction factor takes into account the differences between the current distributions in ridged and plain waveguides. The attenuation constant is negligible in comparison to the electron gain [11].

The field components in Eq. (16) are to be evaluated along the electron orbits. As mentioned in Sec. I the legs where the electron beam crosses the folded waveguide are separated by a distance of l along the z axis, and the electrons experience a periodic electric field E_y with periodicity length l . Since the legs are obtained by bending the waveguide 90° in the xz plane with respect to the beam propagation direction (z axis), the periodic electric field acting on the electrons may be written as [see Eqs. (7) and (8)]

$$E_y(z, t) = \frac{m_0 c^2 A(z)}{eaN} e^{i[\omega t + (-1)^q k_0 x]} \times \begin{cases} \cos(k_c |z|), & 0 < |z| < a_0/2 \\ \frac{b_0}{b} \frac{\cos(\xi_0)}{\sin(\xi_1)} \sin \left[k_c \left[\frac{a}{2} - |z| \right] \right], & a_0/2 < |z| < a/2 \\ 0, & a/2 < |z| < l/2, \end{cases} \quad (19)$$

where $(-1)^q$ accounts for the change in propagation direction in the q th leg of the folded guide. By expanding $E_y(z)$ in a Fourier series, the field may be written as a sum of spatial harmonics as

$$E_y(z) = \sum_{m=-\infty}^{m=+\infty} \frac{m_0 c^2 A(z)}{eaN} F_m e^{-i(\xi+\xi_m)} e^{i\omega t}, \quad (20)$$

where $\xi = \int_0^z k(z') dz'$ and $\xi_m = 2\pi m z / l$. The Fourier transform F_m of the fast varying part of the electric field is given by

$$F_m = \frac{1}{2l} \int_{-l}^l \frac{eaN}{m_0 c^2 A(z)} E_y(z) e^{i(\xi+\xi_m)},$$

i.e.,

$$F_m = F_m^0 \cos(k_0 x) = \frac{a_0}{2l} G_m \cos(k_0 x), \quad (21)$$

where the gap factor G_m is given by

$$G_m = \left[\left\{ \frac{\sin([\bar{k}_m - 1]\xi_0)}{[\bar{k}_m - 1]\xi_0} + \frac{\sin([\bar{k}_m + 1]\xi_0)}{[\bar{k}_m + 1]\xi_0} \right\} + \left\{ Q_+ \frac{\sin([\bar{k}_m - 1]\xi_1/2)}{[\bar{k}_m - 1]\xi_1/2} - Q_- \frac{\sin([\bar{k}_m + 1]\xi_1/2)}{[\bar{k}_m + 1]\xi_1/2} \right\} \right], \quad (22)$$

with

$$\bar{k}_m = k_m / k_c \quad (23)$$

and

$$Q_{\mp} = \frac{b_0(a - a_0)}{ba_0} \frac{\cos\xi_0}{\sin\xi_1} \sin\{\bar{k}_m \xi_0 + (\bar{k}_m \mp 1)\xi_1/2\}. \quad (24)$$

The gap factor for the H -plane-bend folded guide is more complicated than the simple $\sin\xi/\xi$ form for the E -plane-bend rectangular waveguide. From the relation $\nabla \times \mathbf{E} = -\partial \mathbf{B} / \partial t$, the time varying magnetic field associated with the periodic electric field in Eq. (20) may be written as

$$B_x = -\frac{m_0 c^2 A(z)}{ea\omega N} \sum_{m=-\infty}^{m=+\infty} \left\{ \frac{\partial \xi}{\partial z} + \frac{2\pi m}{l} + i\Gamma \right\} \times F_m^0 \cos(k_0 x) e^{-i(\xi+\xi_m)} e^{i\omega t}, \quad (25)$$

$$B_z = -i \frac{m_0 c^2 A(z)}{ea\omega N} \sum_{m=-\infty}^{m=+\infty} k_0 F_m^0 \sin(k_0 x) e^{-i(\xi+\xi_m)} e^{i\omega t}, \quad (26)$$

where $\Gamma = [A(z)]^{-1} dA(z)/dz$ is the growth rate of the radiation amplitude.

From Eqs. (16), (17), (20), and (21), the nonlinear equations for the evolution of the wave phase and amplitude may be written as

$$\left\{ \frac{d^2}{d\bar{z}^2} - \frac{1}{(1+h/l)^2} \left[\frac{d\xi}{d\bar{z}} \right]^2 + (\bar{\omega}^2 - \bar{k}_c^2) \right\} A(z) = -\frac{2\bar{\omega}\bar{I}_0}{N} \left\langle F_m \frac{u_y}{\langle u_{z0} \rangle} \sin\Theta_m \right\rangle, \quad (27)$$

$$\left\{ A(\bar{z}) \left[\frac{d^2 \xi(\bar{z})}{d\bar{z}^2} + \bar{\omega}^2 \tan\delta_l \right] + 2 \frac{dA(\bar{z})}{d\bar{z}} \frac{d\xi}{d\bar{z}} \right\} = \frac{2(l+h/l)\bar{\omega}\bar{I}_0}{N} \left\langle F_m \frac{u_y}{\langle u_{z0} \rangle} \cos\Theta_m \right\rangle, \quad (28)$$

where $\Theta_m = \omega t - \xi - \xi_m$. Equations (27) and (28) have been written in a normalized form which scales out the width a of the waveguide. The dimensionless variables are defined as follows: $\bar{z} = z/a$, $\bar{k} = ka = d\xi/d\bar{z}$, $\bar{\omega} = \omega a/c$, $\bar{t} = ct/a$, $\bar{\Omega} = \Omega a/c$, $\beta_i = v_i/c$, $u_i = \gamma\beta_i$, $\bar{E}_i = eE_i a/m_0 c^2$, $\bar{B}_i = eB_i a/m_0 c$, and $\bar{I}_0 = eI_0/\epsilon_0 m_0 c^3$. The quantities in angular brackets in Eqs. (27) and (28) denote an average over the initial distribution of the electrons in cross section, phase, and velocity.

The nonlinear equations for the electron trajectories may similarly be obtained from Eqs. (15), (20), (21), (26), and (27). Since we are interested in the steady state amplifier operation, the equations will be expressed in terms of axial derivatives instead of time derivatives using the relation $v_z d/dz = d/dt$ along the electron orbits. Thus we obtain

$$\frac{du_x}{d\bar{z}} = -\frac{\beta_y \bar{k}_0 A(z)}{N\beta_z \bar{\omega}} \sin(\bar{k}_0 \bar{x}) \sum_m F_m^0 \sin\Theta_m - \frac{1}{\beta_z} (\beta_y \bar{B}_{0z} - \beta_z \bar{B}_{0y}), \quad (29)$$

$$\frac{du_y}{d\bar{z}} = -\frac{A(z)}{N\beta_z \bar{\omega}} \sum_m F_m^0 \cos(\bar{k}_0 \bar{x}) \left\{ \left[\bar{\omega} - \beta_z \frac{d\xi}{d\bar{z}} - \frac{2\pi m \beta_z}{l} \right] \cos\Theta_m + \beta_z \bar{\Gamma} \sin\Theta_m \right\} + \frac{\beta_x \bar{k}_0 A(z)}{N\beta_z \bar{\omega}} \sum_m F_m^0 \sin(\bar{k}_0 \bar{x}) \sin\Theta_m + \frac{1}{\beta_z} (\beta_x \bar{B}_{0z} - \beta_z \bar{B}_{0x}), \quad (30)$$

$$\frac{du_z}{d\bar{z}} = -\frac{\beta_y A(z)}{N\beta_z \bar{\omega}} \sum_m F_m^0 \cos(\bar{k}_0 \bar{x}) \left\{ \left[\frac{d\xi}{d\bar{z}} + \frac{2\pi m}{l} \right] \cos\Theta_m - \bar{\Gamma} \sin\Theta_m \right\} + \frac{1}{\beta_z} (\beta_y \bar{B}_{0x} - \beta_x \bar{B}_{0y}), \quad (31)$$

and

$$\frac{d\bar{t}}{d\bar{z}} = \frac{1}{\beta_z}, \quad (32)$$

where $\bar{\Gamma} = \Gamma = (dA(\bar{z})/d\bar{z})/A(\bar{z})$ is the normalized growth rate of the wave amplitude. The trajectory equations (27)–(31) for the gyrating electrons include both the guiding center motion and the Larmor rotation about the guiding center. The rate of change of energy of an electron can be obtained from Eqs. (29)–(31) as

$$\frac{d\gamma}{d\bar{z}} = -\frac{\beta_x}{\beta_z} \frac{A(\bar{z})}{N} \sum_m F_m^0 \cos(\bar{k}_0 \bar{x}) \cos\Theta_m. \quad (33)$$

The output power P_{out} in the waveguide can be determined from Eq. (13) by substituting the wave amplitude and wave vector. The efficiency of the amplifier is given by $\eta = (P_{\text{out}} - P_{\text{in}})/V_0 I_0$, where eV_0 is the beam energy ($\gamma = 1 + eV_0/m_0 c^2$) and P_{in} is the input signal power.

IV. RESULTS AND DISCUSSIONS

The set of coupled nonlinear equation in Eqs. (27)–(33) are solved numerically by specifying the initial conditions of the electron beam and the input signal. For the radiation field at $z=0$, we set $k = d\xi/dz = k_0$, $dA/dz = 0$, and $A = (\omega P_{\text{in}}/ck_0 P_N)^{1/2}$, where $P_N = \epsilon_0 m_0^2 c^5 l/2e^2(l+h)$. The initial states of the electrons at $z=0$ are chosen to model the injection of a gyrating monoenergetic beam with uniform distribution in phase and cross section. Although the beam is monoenergetic, it may have a pitch-angle spread specified by the initial distribution function of the form

$$f_0(\mathbf{v}) \propto \exp\left\{-\frac{(v_z - v_{z0})^2}{2(\Delta v_z)^2}\right\} \\ \times \delta(v_1^2 + v_2^2 - v_{10}^2 - v_{20}^2) \delta(\gamma - \gamma_0).$$

The unperturbed dispersion curves for the circuit are shown in Fig. 2. The forward wave dispersion curve for the fundamental space harmonic ($m=0$) is divided into slow and fast wave regions due to the intersection of the light line at a frequency $\omega_{x,c}/\omega_c = (1+l/h)/\sqrt{1+2l/h}$. The frequency band of the amplifier operation will be limited to either the fast or the slow wave region since the beam-wave interaction becomes vanishingly small at frequencies near the light line. The amplifier bandwidth may also be reduced if backward waves are not suppressed. Backward waves at higher order spatial harmonics ($m \geq 1$) intersect the fundamental mode at frequencies $\omega_{x,m}/\omega_c = \sqrt{1 + \{\pi m/k_c(l+h)\}^2}$. Methods for suppression of backward waves will be discussed below.

We first show results of nonlinear calculations for a double-ridged rectangular folded waveguide. The backward waves for higher order spatial harmonics can be widely separated in a double-ridged configuration, and a larger bandwidth can be attained. The parameters of the interaction circuit are $a = 0.3073$ cm (the cutoff frequency is 29.5 GHz), $b/a = 1.5$, $a_0/a = 0.5$, $b_0/b = 0.4$, and $a/l = 0.8$. The beam voltage is 65 kV and the current is

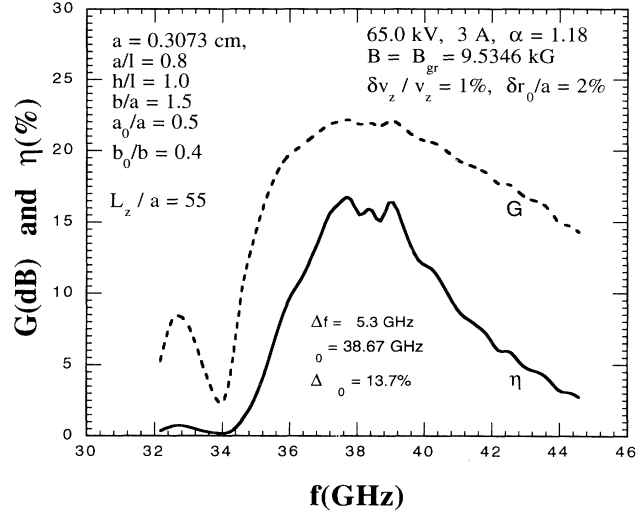


FIG. 3. Plot of gain (dashed curve) and efficiency (solid curve) vs frequency for the TE₁₀ mode at a guide magnetic fields $B_0/B_{\text{gr}} = 1.0$ for $\alpha = 1.18$, $\delta r_0/a = 2\%$, and $\delta v_z/v_{z0} = 1\%$. The circuit parameters are $b/a = 1.5$, $a_0/a = 0.5$, $b_0/b = 0.4$, $a/l = 0.8$, $h/l = 1.0$, and $a = 0.3073$ cm. The beam voltage is 65 kV, the current is 3 A, and the interaction length $L = 55a$.

3 A. The input signal power is 200 W. The parameters correspond to an experiment underway at Naval Research Laboratory (NRL). Calculations are done for a wide range of axial guide magnetic field B_0 , velocity ratio $\alpha = \beta_{10}/\beta_{20}$, axial beam velocity spread $\delta v_z/v_{z0}$, guiding center spread $\delta r_0/a$, and phase velocity slowing parameter h/l . Results are presented for the operation in the fundamental spatial harmonic ($m=0$) of the TE₁₀ mode interacting with the fundamental cyclotron harmonic ($s=1$).

The gain and efficiency are shown as functions of frequency in Fig. 3 for $h/l = 1.0$, $\alpha = 1.18$, $\delta v_z/v_{z0} = 1\%$, and $\delta r_0/a = 2\%$. The interaction length is $L = 55a = 16.90$ cm. The uniform guide magnetic field B_0 is 9.5364 kG. The magnetic field corresponds to the grazing condition, i.e., $\Omega_0 = eB_0/m_0 = \gamma \omega_c \sqrt{1 - (1+h/l)^2 \beta_z^2}$ for the reduced dispersion waves. In this circuit, the light-line intersection is at $f_{x,c} = 34.07$ GHz (the slow and fast wave regions are, respectively, above and below 34.07 GHz). The $m = 1$ and 2 backward wave intersections are, respectively, at frequencies 35.37 and 48.92 GHz. The backward wave at 35.37 GHz can be eliminated by using the mode coalescing technique [10]. The values of α and h/l were chosen to maximize the bandwidth in the slow wave region. As expected, the beam-wave interaction is very weak at frequencies where $v_{\text{ph}} \approx c$. The instantaneous 3-dB bandwidth (i.e., full width at half maximum) $\Delta f/f_0 = 13.7\%$ with a center frequency $f_0 = 38.65$ GHz. (The frequency range is 36.0–41.3 GHz.) The maximum gain is 22.1 dB (the maximum efficiency is 16.63%) at 37.8 GHz. The evolution of the radiation power (watts) and growth rate $\Gamma = A^{-1} dA/dz$ as functions of axial position are shown in Figs. 4(a) and 4(b), respectively, at a frequency of 37.8

GHz. Saturation was found at $z = 55a$ with a power of 30.487 kW. The growth of the wave is approximately exponential after an initial insertion loss region $z/a < 15$. During the linear stage of the interaction, the growth rate is about 2 dB/cm, in agreement with the linear theory. The effect of a beam axial velocity spread on the amplifier operation is shown in Figs. 5(a) and 5(b), where gain and efficiency are plotted as functions of frequency for several values of $\delta v_z/v_z$ with $\delta r_0/a = 0$. The peak efficiency drops rapidly from 25.87% to 5.65% as $\delta v_z/v_z$ is increased from 0% to 2%. The bandwidth is less sensitive to the velocity spread and increases from 12% to 16%. The variation of gain and efficiency with guiding center spread of the electrons is shown in Figs. 6(a) and 6(b) for $\delta v_z/v_z = 0$. There is practically no change in efficiency, gain, and bandwidth for $\delta r_0/a$ up to 2% (i.e.,

$\delta r_0/r_L \sim 9.5\%$). Beam interception occurs as $\delta r_0/a$ increases from 2% to 5%, and the peak efficiency decreases from 25.87% to 11.72% while the bandwidth increases from 11% to 18%. From Eqs. (27), (28), and (33), it is seen that the beam-wave coupling depends on the electron guiding center location through a $\cos(\kappa_0 x)$ term in the Fourier transform F_m [Eq. (21)] of the radiation electric field. The coupling strength changes very slowly with x_0 for $\kappa_0 x < 1$, where $x = x_0 + r_L \cos\psi$. The guiding center coordinates are denoted by x_0 , and y_0 , and the rotation about the guiding center is described by a Larmor radius r_L and gyrophase ψ . In the present case, the initial Larmor radius $r_L(0)$ is $0.23a$, and the half-width $b_0/2$ of the ridge in the y direction is $0.3a$. As the interaction proceeds, some of the electrons reach the waveguide wall as $\delta r_0/a$ increases above 2%.

In the next example, we consider a circuit which has

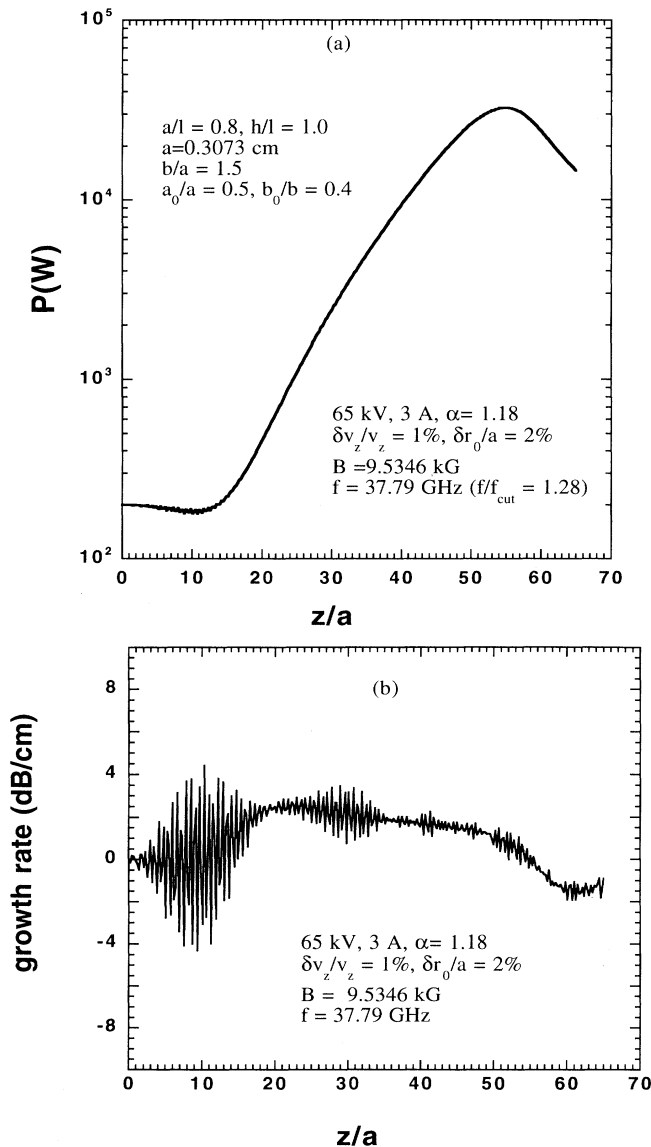


FIG. 4. Evolution of (a) radiation power and (b) growth rate as functions of axial position at a frequency of 37.8 GHz.

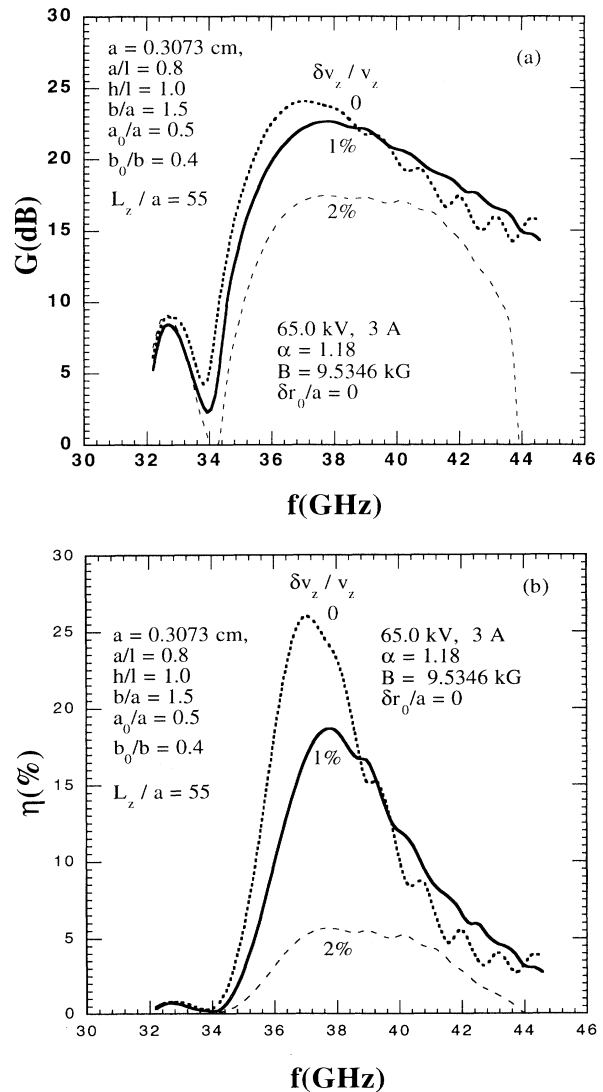


FIG. 5. Graph of (a) gain and (b) efficiency vs frequency for three values of $\delta v_z/v_z = 0, 1\%$, and 2% with $\delta r_0/a = 0$. All other parameters are the same as in Fig. 3.

the same parameters as the previous case except $h/l=0.6$, $\alpha=1.2$, and $B_0=10.4706$ kG. These parameters are suitable for optimization of the fast wave region. The fast and the slow wave regions are separated at 37.8 GHz, and the $m=1$ backward wave intersection occurs at 38.28 GHz. The gain and efficiency as functions of frequency in the fast wave region are shown in Fig. 7 for $\delta v_z/v_z=2\%$ and $\delta r_0/a=2\%$. The interaction length is $L=52a$. The bandwidth is 9.5%, with a center frequency at 31.68 GHz (frequency range 30.18–33.18 GHz). The maximum gain is 26.16 dB with 42.4% efficiency at 30.41 GHz. The output power is 82.72 kW. Due to stronger interaction, the fast wave region has higher efficiency and gain and is also less sensitive to deviations from the ideal beam conditions compared to the slow

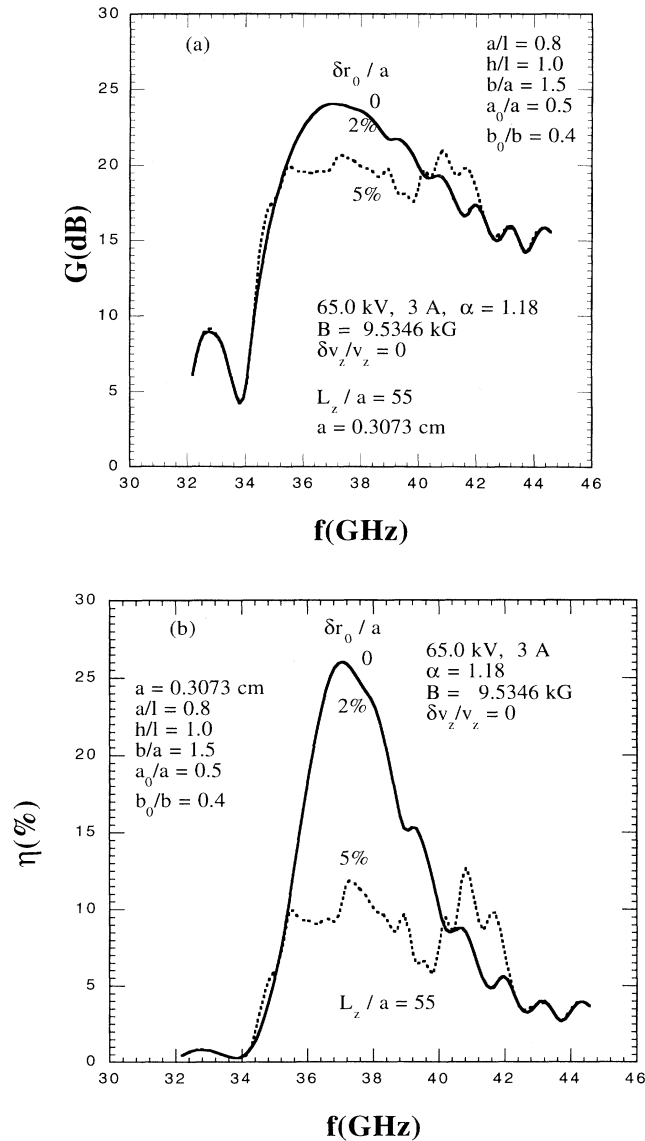


FIG. 6. Plots of (a) gain and (b) efficiency vs frequency for $\delta r_0/a=0, 2\%$, and 5% at $\delta v_z/v_{z0}=0$. Other parameters are the same as in Fig. 3.

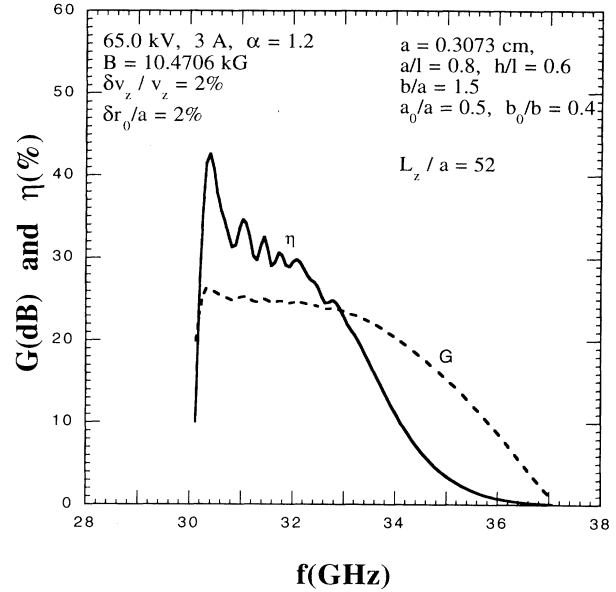


FIG. 7. Plot of gain (dashed curve) and efficiency (solid curve) vs frequency for $B_0/B_{gr}=1.0$, $\alpha=1.2$, $\delta r_0/a=2\%$, and $\delta v_z/v_{z0}=2\%$. The circuit parameters are $b/a=1.5$, $a_0/a=0.5$, $b_0/b=0.4$, $a/l=0.8$, $h/l=0.6$, and $a=0.3073$ cm. The beam voltage is 65 kV, the current is 3 A, and the interaction length $L=52a$.

waves. However, the bandwidth is smaller since the fast waves are more dispersive. The dependence of gain, efficiency, and bandwidth on velocity spread are shown in Figs. 8(a) and 8(b) for $\delta r_0/a=0$. In the case of fast waves, the bandwidth also decreases with increase in velocity spread. From Figs. 8(a) and 8(b), it is seen that the peak efficiency drops from 44% to 36% as $\delta v_z/v_z$ increases from 0% to 4%, and the bandwidth decreases from 11.5% to 6%. The effects of the guiding center spread on the fast wave amplifier operation [Figs. 9(a) and 9(b)] are similar to those of the slow waves. The gain efficiency and bandwidth show little change up to $\delta r_0/a$ of about 2%. The electron beam has an initial radius $r_L(0)=0.21a$, and the amplifier operation deteriorates with further increase in $\delta r_0/a$ due to beam interception. At $\delta r_0/a=4\%$, the peak efficiency drops to 27.1% with 24.2-dB gain, but the bandwidth increases to 13.4%.

Next we consider an unridged waveguide. Fabrication of unridged structures is easier, but the bandwidth will be smaller compared to the ridged structures. Results are shown for a 61.5-kV, 3-A, $\alpha=1.2$ electron beam injected into a waveguide of width $a=0.4555$ cm with $b/a=0.67$, $h/l=0.6417$, and $a/l=0.6519$. The cutoff frequency is 32.908 GHz, and the light-line intersection is at 41.494 GHz. The $m=1$ and 2 backward wave intersections occur at 35.40 and 42.02 GHz, respectively. Calculations were performed in the fast wave region (32.91 GHz $< f < 41.49$ GHz) with a guide magnetic field $B_0=11.5984$ kG. Gain and efficiency are plotted as functions of frequency in Figs. 10(a) and 10(b), respective-

ly, at different values for the axial beam velocity spread with $\delta r_0/a=0$. The interaction length is $L=45a$. The peak efficiency decreases from 44% to 26% as $\delta v_z/v_z$ increases from 0 to 4% and the bandwidth decreases from 8.9% to 4.4%. The mode coalescing method [10] or multistage operation will be required to suppress the $m=1$ backward wave. There is practically no change in the amplifier performance when $\delta r_0/a$ is increased from 0 to 0.15 (i.e., $0 < \delta r_0/r_L < 1.2$). Since $r_L(0)/a=0.12$ and $b/2a=0.33$, there is no beam interception even at large guiding center spread.

V. CONCLUSIONS

A nonlinear theory of slow wave cyclotron interaction in a rectangular folded waveguide has been developed.

An H -plane-bend configuration is used to increase the power handling capability compared to the conventional E -plane-bend waveguides. The bandwidth in an E -plane-bend circuit, however, is larger since the light line does not cross the $m=0$ forward wave branch due to an additional phase shift of π between the legs of the bend. Calculations have been performed for both unridged and double ridged waveguides. A double-ridged waveguide can produce greater separation of the space harmonics and gives larger bandwidth. The gain, efficiency, and bandwidth are very sensitive to the beam axial velocity spread. For broadband amplification, $\delta v_z/v_z < 2\%$ in the fast wave region and $\delta v_z/v_z < 1\%$ in the slow wave region. The amplifier performance is insensitive to the guiding center spread unless beam interception occurs. In an unridged structure, no degradation of performance

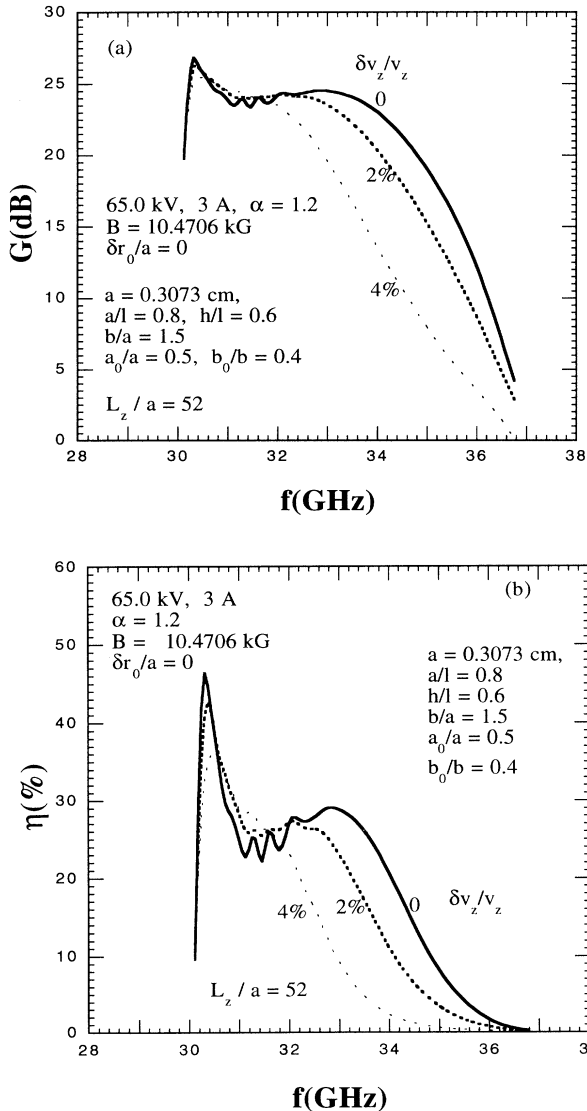


FIG. 8. Graph of (a) gain and (b) efficiency vs frequency for three values of $\delta v_z/v_z=0, 2\%$, and 4% with $\delta r_0/a=0$. All other parameters are the same as in Fig. 7.

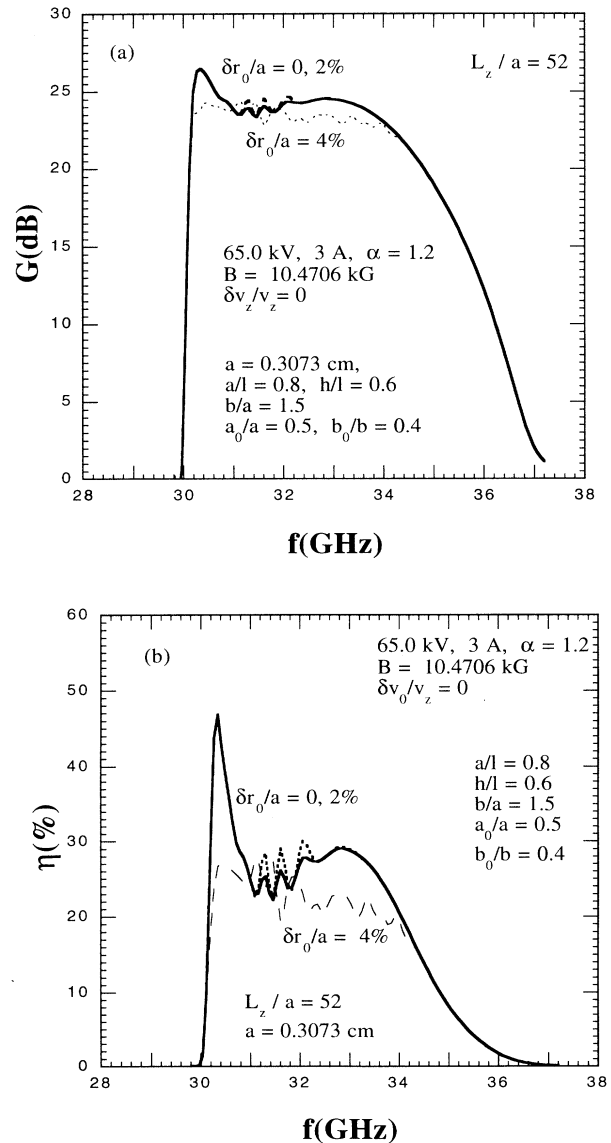


FIG. 9. Plots of (a) gain and (b) efficiency vs frequency for $\delta r_0/a=0, 2\%$, and 4% at $\delta v_z/v_z=0$. Other parameters are the same as in Fig. 7.

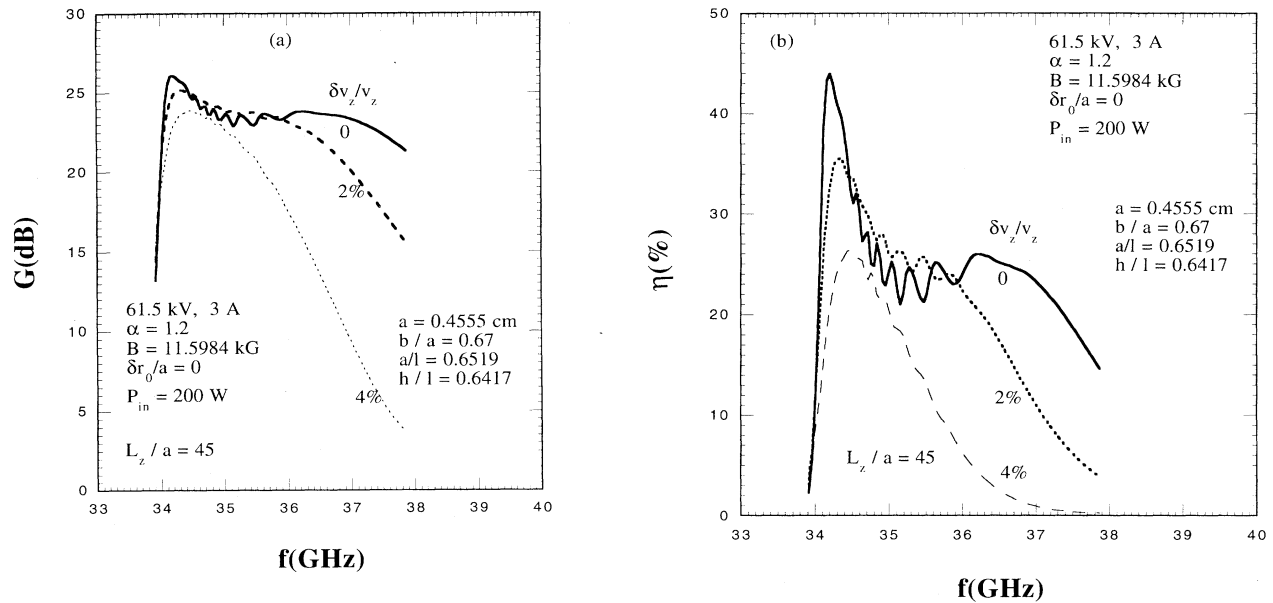


FIG. 10. Plot of gain (dashed curve) and efficiency (solid curve) vs frequency for $B_0/B_{gr} = 1.0$, $\alpha = 1.2$, $\delta r_0/a = 0$, and $\delta v_z/v_{z0} = 0$. The circuit parameters are $b/a = 0.67$, $a/l = 0.6519$, $h/l = 0.6417$, and $a = 0.4555$ cm. The beam voltage is 61.5 kV, the current is 3 A, and the interaction length $L = 45a$.

occurs for $\delta r_0/r_L \sim 1$. In a ridged structure, however, $\delta r_0/r_L$ is limited to less than 10% due to beam interception on the narrow side of the ridge. The slow wave amplification is possible at an efficiency of 16% with 14% bandwidth, and the fast waves have a higher efficiency of 42% and a smaller bandwidth of 10%. The Ohmic loss in the circuit for the TE_{10} mode is negligible compared to the electronic gain. Precautions should be taken to prohibit the backward wave oscillations. Backward

wave oscillations may be suppressed either by using a multistage configuration or by applying the mode coalescing method where the impedance of the beam hole is matched with the impedance of the bends.

ACKNOWLEDGMENTS

The work was supported by ONR and ARPA.

- [1] A. K. Ganguly and S. Ahn, *Phys. Rev. A* **42**, 3544 (1990).
- [2] J. Y. Choe and H. S. Uhm, *Int. J. Electron.* **53**, 729 (1982).
- [3] E. Jerby and G. Bekefi, *Phys. Rev. E* **48**, 4637 (1993).
- [4] G. S. Park, S. Y. Park, R. H. Kyser, C. M. Armstrong, A. K. Ganguly, and R. K. Parker, *IEEE Trans. Plasma Sci.* **22**, 1 (1994).
- [5] J. J. Choi, A. K. Ganguly, and C. M. Armstrong, *Phys. Plasmas* **1**, 2058 (1994).
- [6] G. S. Park, J. J. Choi, S. Y. Park, C. M. Armstrong, A. K. Ganguly, R. H. Kyser, and R. K. Parker, *Phys. Rev. Lett.* **74**, 2399 (1995).
- [7] K. C. Leou, D. B. McDermott, and N. C. Luhman, Jr., *IEEE Trans. Plasma Sci.* **20**, 188 (1992).
- [8] K. C. Leou, D. B. McDermott, F. V. Hartemann, C. K. Chong, and N. C. Luhmann, Jr., *IEEE Int. Electron Devices XX*, 359 (1993).
- [9] G. Dohler, D. Gallagher, and J. Richards (private communication).
- [10] J. J. Choi, C. M. Armstrong, A. K. Ganguly, and F. Calise, *Phys. Plasmas* **2**, 915 (1995).
- [11] A. K. Ganguly, J. J. Choi, and C. M. Armstrong, *IEEE Trans. Electron Devices* **42**, 348 (1995).
- [12] S. Hopfer, *IRE Trans. Microwave Theory Tech.* **MTT-3**, 20 (1955).
- [13] S. B. Cohen, *Proc. IRE* **35**, 783 (1947).
- [14] R. G. E. Hutter, *Beam and Wave Electronics in Microwave Tubes* (Van Nostrand, Princeton, NJ, 1960), pp. 114–120.
- [15] A. K. Ganguly and J. L. Hirshfield, *Phys. Rev. E* **47**, 4364 (1993); *Phys. Rev. Lett.* **70**, 291 (1993).
- [16] N. Marcuvitz, *Waveguide Handbook*, M.I.T. Rad. Lab. Series Vol. 10 (MIT, Cambridge, MA, 1951), pp. 399–402.
- [17] R. E. Collin, *Field Theory of Guided Waves* (McGraw-Hill, New York, 1960), pp. 338–346.